Chemical Physics Letters 575 (2013) 54–58

Contents lists available at SciVerse ScienceDirect

Chemical Physics Letters

journal homepage: www.elsevier.com/locate/cplett

Effects of cage type and adsorption face on the cage–methane adsorption interaction: Implications for hydrate nucleation studies

Chan-Juan Liu, Zheng-Cai Zhang, Zhi-Gang Zhang, Yi-Gang Zhang, Guang-Jun Guo *

Key Laboratory of the Earth's Deep Interior, Institute of Geology and Geophysics, Chinese Academy of Sciences, Beijing 100029, PR China

ARTICLE INFO

Article history:
Received 10 February 2013
In final form 7 May 2013
Available online 16 May 2013

ABSTRACT

The adsorption interaction between a water cage and a methane molecule, shown by the cage–methane PMF (potential of mean force), is key to understanding hydrate formation mechanisms. We investigate how the cage type and adsorption face affect the PMF. The PMF is found to depend on the face size rather than the cage type, and the adsorption interaction becomes stronger as the face size increases. However, once the face becomes 7-membered, it no longer adsorbs methane but allows methane crossing it to enter the cage. The results suggest that a preferential direction may exist during hydrate nucleation and growth.

1. Introduction

Gas hydrates are crystalline compounds consisting of a hydrogen-bonded network of polyhedral water cavities (the hosts) that encage small gas molecules (the guests), and methane hydrate is a prototype. Because methane hydrate is abundant in permafrost regions and the seafloor of continental margins, it is considered to be a potential energy resource [1,2]. Methane hydrate is also important for flow assurance in the oil and gas industry and in the environment for global warming. In hydrate research fields, the molecular mechanism of methane hydrate formation is a fundamental issue relating to many still open topics, such as stochastic nucleation [1,3–4], the memory effect [5,6], and structural transition [7,8]. Early studies on the hydrate nucleation mechanism mainly include the labile cluster hypothesis (LCH) proposed by Sloan and co-workers [1,9], which emphasized the aggregation of cage-like water clusters, and the local structuring hypothesis (LSH) proposed by Radhakrishnan and Trout [10], which emphasized the adjustment of water molecules around a local, ordered arrangement of gas molecules. Recently, Guo and co-workers [11] proposed the cage adsorption hypothesis (CAH), in which the cage–methane adsorption interaction is the inherent driving force controlling hydrate formation. The CAH also predicts that an intermediate amorphous hydrate phase should occur before the final crystalline hydrate forms, which is supported by the MD simulations of methane hydrate formation [12,13], and by the two-step mechanisms of hydrate formation [14,15].

In this Letter, we focus on the adsorption interaction between a water cage and a methane molecule. Given a water cage formed in a methane aqueous solution, when a dissolved methane molecule approaches the cage, the cage will adsorb the methane on one of its faces. This is considered to be a favorable step in triggering a hydrate nucleation event because the adsorbed methane can prolong the cage's lifetime and induce a new cage to form around it [16]. If the cage is located on the hydrate surface in contact with the methane solution, the step will also favor the crystal growth for the same reason. In our previous work [11], we studied the cage–methane adsorption interaction by calculating the potential of mean force (PMF) between a dodecahedral cage (5^{12}) and a methane molecule, and considered three influencing factors: the rigidity, filling status, and orientation of the cage. The main finding was that the strength of the attractive interaction between the cage and methane was comparable to the strength of hydrogen bonds. A rigid cage led to a slightly stronger adsorption interaction than a soft cage, while the filled cage with a methane molecule was no different from an empty cage. Additionally, the cage's adsorption interaction showed a kind of directionality, with the strongest interaction points oriented toward the center of the adsorption face and perpendicular to this face.

However, because just the 5^{12} cage, which has only pentagonal faces, was used in the previous work, the effects of cage type and face size on the cage–methane adsorption interaction could not be studied. These two factors are very important and should be examined carefully. Regarding the former, thousands of types of cages can occur during hydrate formation [17], and hydrate nuclei need not develop only from the 5^{12} cage initially. Regarding the latter, the size of the cage faces determines whether the methane is adsorbed on one of the cage faces or enters the cage through the face. Although it is taken for granted that a methane molecule can passage a heptagonal (or larger) face but not a hexagonal (or smaller) face, no direct evidence exists in the literature. This point is also of significance for studies on the inter-cage diffusion of guests in hydrate, especially in amorphous-phase hydrate that

* Corresponding author. Fax: +86 10 82998369.
E-mail address: guogj@mail.igcas.ac.cn (G.-J. Guo).

0009-2614/$ - see front matter © 2013 Elsevier B.V. All rights reserved.
http://dx.doi.org/10.1016/j.cplett.2013.05.012

can occur during the intermediate stage of hydrate formation [14–15,17], and the structural transition of hydrate caused by high pressure [18,19]. Therefore, in this work we study how the cage type and the size of the adsorption face affect the cage–methane adsorption interaction.

2. Method

All molecular dynamics simulations were carried out using the GROMACS package [20,21]. The system was designed as a cuboid of $45 \times 30 \times 30$ Å ($x \times y \times z$), consisting of one cage, two methane molecules, and 1240 water molecules. The water molecules were described by the TIP4P/2005 potential model [22] and the methane by the OPLS-UA potential [23]. The cross interactions between water and methane were calculated according to the modified Lorentz–Berthelot combining rules (with $\chi = 1.07$) [24]. The Nosé–Hoover thermostat and Parrinello–Rahman barostat, with a period of 0.8 ps for both, were used to obtain the NPT ensemble with a temperature of 258.5 K and a pressure of 30 MPa, with a state point located in the methane hydrate phase region for the above potential models [25]. The cutoff distance was 10 Å for the Lennard–Jones potential. Periodic boundary conditions were used in all directions and the long-range interaction was calculated using the particle mesh Ewald method with a real space cutoff of 10 Å, spline order of 4, and Fourier spacing of 1.2 Å. In total, eight representative cages containing five types of faces (Figure 1) were used to check the effects of the cage type and the face size on the cage–methane adsorption interaction. The cages were all extracted from the MD trajectories for hydrate formation reported by Walsh et al. [13] using our face-saturated incomplete cage analysis [17]. The edge length of these cages was set as 2.82 Å (i.e., the average length of H-bonds), which is slightly larger than the previously used value of 2.75 Å [11].

To study the cage–methane adsorption interaction, similar to the method used in our previous work [11] we used constrained molecular dynamics simulations to calculate the potential of mean force (PMF) between a cage and a methane molecule. It is possible to constrain the distance between the cage and the methane at r_c during simulations, and then calculate the constraint mean force $F(r_c)$ exerted on them. Thus, the cage–methane PMF is equal to the integration of $F(r_c)$; that is,

$$\mathrm{PMF}(r_2) - \mathrm{PMF}(r_1) = -\int_{r_1}^{r_2} F(r_c)dr_c, \tag{1}$$

where r_1 is the constrained distance of the reference state and r_2 is an arbitrary constrained distance. For convenience, r_1 often takes a value large enough so that $\mathrm{PMF}(r_1)$ reaches zero. Therefore, the PMF can be calculated from

$$\mathrm{PMF}(r_2) = -\int_{r_1}^{r_2} F(r_c)dr_c. \tag{2}$$

In addition, because of the above constraint condition, the rotation of the combination of cage and methane will produce an entropy contribution to the PMF [21]. This should be corrected by subtracting $2k_BT/r_c$ from the original output of $F(r_c)$ in GROMACS [11]. According to the above definition, the cage–methane PMF is actually the free energy along the reaction coordinate, r_c. Using it, we can obtain the radial distribution function (RDF) by

$$\mathrm{RDF}(r) = e^{-\mathrm{PMF}(r)/k_BT}, \tag{3}$$

where k_B is the Boltzmann constant and T is the system temperature. It is not possible to calculate the cage–methane RDF directly from the MD simulations due to the problem of poor sampling, and the relevant discussion can be found elsewhere [11].

To perform the constrained MD simulations, we first defined two groups – the adsorption face and the dissolved methane. The definition of the first group differs from that in our previous work, in which the whole cage was defined as a group. The current definition removes the influence of different distances from the cage center to the different face centers on the PMF, thus enabling us to conveniently compare different PMF curves. Nevertheless, because the present definition shifts the origin of r_c from the cage center to the face center by Δr_c (= 3.1 Å for the 5^{12} cage), the difference must be considered when comparing the present and the previous PMF. Then, we placed the two groups on the x-axis in the middle of the simulation box, with the adsorption face of the cage perpendicular to the x-axis. During the simulation, the two groups could move freely but their separation was fixed at r_c. To ensure the cage face was always perpendicular to the straight line linking the face center and the dissolved methane, we additionally constrained all N_v numbers of distances between every face vertex and the dissolved methane to be equal, where N_v is the number

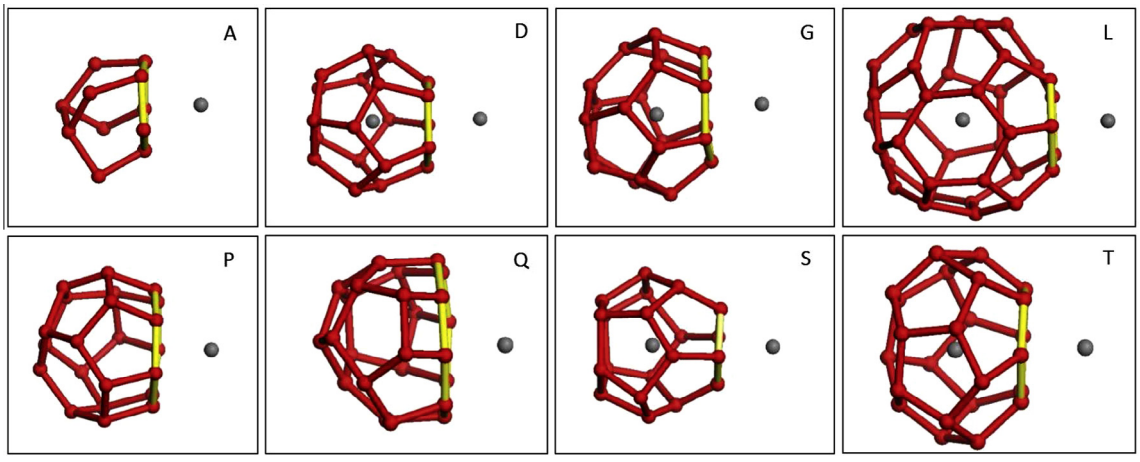

Figure 1. The different cages used in this work. The red balls are water oxygen and the gray balls are methane. The sticks are H-bonds, in which the yellow sticks indicate the adsorption face to the dissolved methane. The cage names are shown in the top right corners, respectively, and are described as follows. (A) $[5^26^3]_5$ cage, the most abundant cage in the methane solution prior to hydrate nucleation [17]. According to our previous notation, $[\ ]_5$ indicates that it is an incomplete cage with five vertices with only two shared edges for each. (D) 5^{12} cage, the most common cage in hydrates. (G) $4^15^{10}6^2$ cage, which contains 4-, 5-, and 6-membered faces and is very abundant during hydrate nucleation. (L) $5^{12}6^8$ cage, an example of a large cage. (P) $4^35^76^27^1$ cage containing a 7-membered face. (Q) $4^45^66^38^1$ cage containing an 8-membered face. (S) $4^35^66^3$ cage, a small cage containing 4-, 5-, and 6-membered faces. (T) $5^{12}6^2$ cage, the main cage in the sI hydrate.

of face vertices. We used the SHAKE algorithm and the COM pulling codes of GROMACS to output the constraint force of the two groups. Each simulation was run for 602 ps. The initial 2 ps were run using a small step of 0.2 fs to relax the system smoothly, and the following 600 ps were run using the usual step of 1 fs. We checked that the combination of cage and methane seldom crossed the system boundary during the 602 ps-long simulations. The data from the last 500 ps were used to obtain the mean force $F(r_c)$. Here, r_c comprised 56 sample points, varying from 1 Å to 12 Å with an interval of 0.2 Å, and PMF (12 Å) was set at zero (see Eqs. (1) and (2)). Compared to the previous PMF-cutoff of 10.9 Å (= 14 Å − Δr_c) [11], the present cutoff (= 12 Å) was rather conservative. To obtain accurate statistics, we performed 20 independent simulations for each sampling point, thus ensuring that the $F(r_c)$ were averaged over 10 ns-long configurations.

Similar to our previous work, either rigid or soft cages were used in different case studies. The rigid cages were achieved by exerting both distance constraints and angle constraints on the membered water molecules, while the soft cages were achieved by exerting only distance constraints. For the distance constraints, the length of the OH bond in water molecules was set at 0.9572 Å, the H–H distance at 1.5139 Å, the O–M distance at 0.1546 Å, the H–M distance at 0.8712 Å, and the length of H-bonds at 2.82 Å. For the angle constraints, the angle between three neighboring O atoms in a cage face was set at $180^\circ \times (N_v - 2)/N_v$. To simulate the real situation of a cage in bulk water, we set all cages as soft, and filled them with a methane guest if possible. However, we set the cages with 7- and 8-membered water rings as rigid, otherwise these cages would collapse during simulations.

We calculated 18 cases of the cage–methane PMF: $SA[0]_{F5}M$, $SA[0]_{F6}M$, $SD[M]_{F5}M$, $SG[M]_{F4}M$, $SG[M]_{F5}M$, $SG[M]_{F6}M$, $SL[M]_{F5}M$, $SL[M]_{F6}M$, $SS[M]_{F4}M$, $SS[M]_{F5}M$, $SS[M]_{F6}M$, $ST[M]_{F5}M$, $ST[M]_{F6}M$, $RG[0]_{F4}M$, $RG[0]_{F5}M$, $RG[0]_{F6}M$, $RP[0]_{F7}M$, $RQ[0]_{F8}M$. In this notation, [ ] is used to represent a polyhedral cage whose appearance is described by the characters on the left side of [ ]. R represents a rigid cage and S a soft one, while the second letter is the name of the cage, as listed in Figure 1. Guests lie within [ ], with M and 0 denoting methane and the absence of methane, respectively. On the right side of [ ], M is the dissolved methane and the subscripts F4, F5, F6, F7, and F8 refer to tetragonal, pentagonal, hexagonal, heptagonal, and octagonal faces respectively, which describe the orientation of the cage relative to the dissolved methane.

3. Results

3.1. The effect of different cage types on PMF

Figure 2 shows the cage–methane PMFs for the cases $SA[0]_{F5}M$, $SD[M]_{F5}M$, $SG[M]_{F5}M$, $SL[M]_{F5}M$, $SS[M]_{F5}M$, and $ST[M]_{F5}M$. All of these cases have the pentagonal face orientation. The figure shows that the PMFs are almost the same for all of the cages except $SA[0]_{F5}M$. There is a very deep well at 2.8 Å, with a value of −15.2 kJ/Mol. For all cages except the empty A cage, the first barrier is located at ~5.6 Å and the second well is located at 7.6 Å. The result agrees well with our previous work, in which the three characteristic distances were 2.9, 5.7, and 7.1 Å (after subtracting the Δr_c of 3.1 Å) [11]. The PMF curve for the $SA[0]_{F5}M$ case also shows the same feature in the first well, but its second well is much closer than in other cases. Because the A cage, $[5^2 6^3]_5$, is a small incomplete cage, the phenomenon may indicate that it is less capable of making extended cage-like structures than the large complete cages. The PMF results for the tetragonal and hexagonal faces of different cages are also shown in Supplementary Figures S1 and S2, respectively. Similar to the situation for the pentagonal face, no conspicuous difference is observed between different cage

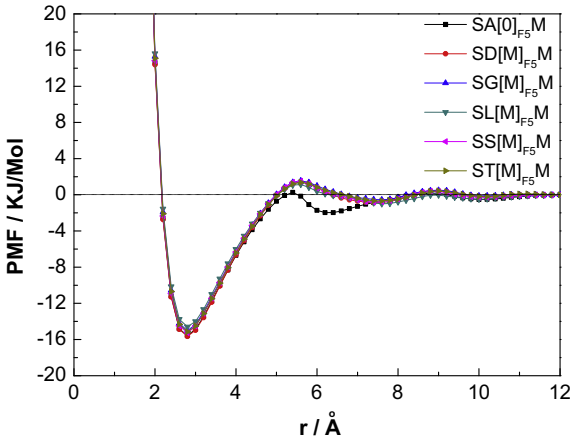

Figure 2. The cage–methane PMFs for the pentagonal adsorption face. The error bars are covered by the labels.

types except for the A cage. We also examined the effect of the position of the cage face on the PMF. Three pentagonal faces located at different positions on the G cage ($4^1 5^{10} 6^2$) were selected to calculate the PMF, and the results were the same (not shown here for brevity). Finally, we examined the effect of cage types on PMF using another potential combination of water and methane, which gives a more accurate cross interaction based on *ab initio* simulations [26] and was previously used in a study on the PMF between the 5^{12} cage and the water/methane interface [27]. The PMF results (Supplementary Figure S3) show some more visible but still small differences between cage types. The L cage shows a slightly weaker attraction to methane than the D cage, and the A cage shows the weakest among the three. The above results show that provided the adsorption faces are of the same size, it is almost unnecessary to consider the cage type and the cage face's position when studying the cage–methane adsorption interaction. However, the incomplete A cage indeed shows a slightly weaker attraction to methane than the other complete cages.

3.2. The effect of different cage faces on PMF

We chose the $4^1 5^{10} 6^2$ and $4^3 5^6 6^3$ cages to examine whether different cage faces affect the cage–methane PMF because both of them have tetragonal, pentagonal, and hexagonal faces. Figure 3 shows the PMF curves for the $4^1 5^{10} 6^2$ cage (i.e., $SG[M]_{F4}M$,

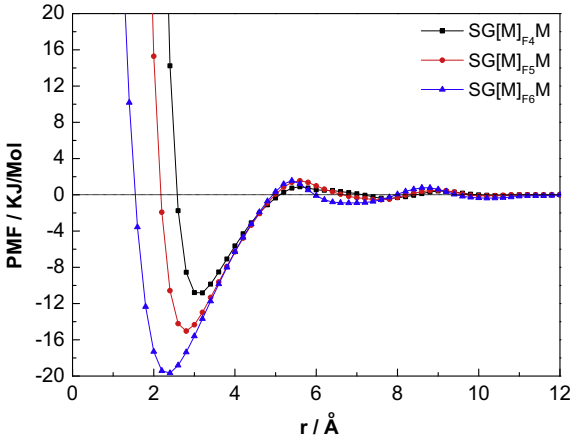

Figure 3. The cage–methane PMFs for different adsorption faces in the G cage, $4^1 5^{10} 6^2$.

$SG[M]_{F5}M$ and $SG[M]_{F6}M$). Because those for the $4^35^66^3$ cage (i.e., $SS[M]_{F4}M$, $SS[M]_{F5}M$ and $SS[M]_{F6}M$) almost coincide with the curves in Figure 3, we do not show them here for clarity. Figure 3 shows that the different cage faces strongly influence the PMF. As the face size increases, the first well becomes closer to the adsorption face and deeper in depth, indicating stronger cage–methane adsorption. Usually, the activation energies (E_a), the free energy difference between the first well and the first barrier to the PMF, can be used to quantify the cage–methane adsorption. Table 1 shows that in all cases, the E_a is larger than the E_a of an H-bond (about 10 kJ/mol) [28]. Moreover, there exists a linear relationship between the E_a and the face size (Figure 4). From the tetragonal to the hexagonal faces, the slope shows that an increment of one vertex stabilizes the adsorption by 4.8 kJ/mol. Considering the E_a for the hexagonal face is more than twice that of an H-bond, the cage–methane adsorption interaction can indeed act as the driving force behind the concentration of methane in its dilute solutions.

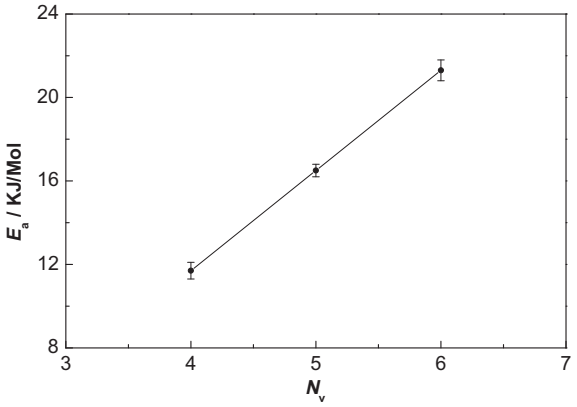

Figure 4. The activation energies (E_a) of cage-adsorbing methane change with the face size (N_v).

3.3. PMF for the cages with large faces

To understand why the dissolved methane can enter the cage with large faces, we calculated the PMFs for the $RP[0]_{F7}M$ and $RQ[0]_{F8}M$ cases with r_c ranging from −3 Å to 12 Å. Here, the negative value indicates that the dissolved methane is initially located on the left side of the adsorption face, i.e., the inside of the cage. The P cage ($4^35^76^27^1$) has a heptagonal face and the Q cage ($4^45^66^38^1$) has an octagonal face (Figure 1). Here, we used the rigid empty P and Q cages during performing simulations with considering the following limits. First, the guest methane filled in advance could have escaped out of the P and Q cages during the simulations, so we had to leave these cages empty. Second, the soft empty P and Q cages could have collapsed during the simulations, so we had to set them as rigid cages to maintain their shapes. Correspondingly, we used the rigid empty $4^15^{10}6^2$ cage to calculate the PMFs of $RG[0]_{F4}M$, $RG[0]_{F5}M$, and $RG[0]_{F6}M$ for comparison. In Figure 5, the PMF results show that the PMF curves for 7- and 8-membered faces are quite different from those for 4-, 5-, and 6-membered faces. The anticipated first well for $RP[0]_{F7}M$ is now located at 1.6 Å, and the repulsive section on its left side degenerates to a low barrier very close to the center of the adsorption face. In the case of $RQ[0]_{F8}M$, the low barrier even disappears completely. The deep wells around −2.0 Å represent the stable positions where methane entered the P and Q cages.

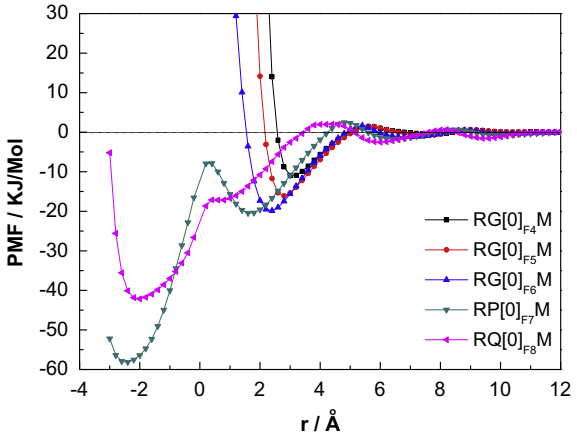

Figure 5. The cage–methane PMFs for the P and Q cages with large faces, compared to the PMF for the G cage.

4. Discussion

The present results indicate that when cages adsorb methane, the strength of the adsorption interaction depends more on the size of the adsorption face than on the cage type, and the attractive force becomes stronger as the face size increases. Therefore, it is highly probable that a cage (except 5^{12}) formed in a methane solution will adsorb dissolved methane molecules on its large faces rather than its small faces. Taking the cage as a template, it is then easier to form a new cage around the methane adsorbed on a large face than on a small face. Therefore, we infer that a preferential direction may exist during hydrate nucleation and growth, and it may be used to explain the morphology of methane hydrate, such as its needle-like and spiral crystals [29], in the future. However, if the face size reaches 7 members or larger, the adsorption faces can no longer adsorb methane. While the 8-membered face is large enough for methane to pass through it smoothly, the 7-membered face presents a zigzag pathway due to the low PMF-barrier located at the face center (Figure 5).

In our previous work [17], we established the face-saturated incomplete cage analysis (FSICA), which can identify all types of face-saturated cages. In this method, a fundamental (but empirical) definition is that the 3-, 4-, 5-, and 6-membered water rings are called cage faces, and the 7- and larger membered water rings

Table 1
Features of the PMF between the $4^15^{10}6^2$ cage and the dissolved methane.[a]

Case	The first well		The first barrier		The second well		E_a (kJ/Mol)
	r (Å)	PMF(r) (kJ/Mol)	r' (Å)	PMF(r') (kJ/Mol)	r'' (Å)	PMF(r″) (kJ/Mol)	
$SG[M]_{F4}M$	3.2	−10.8	5.6	0.9	7.8	−0.4	11.7 ± 0.4
$SG[M]_{F5}M$	2.8	−15.0	5.6	1.5	7.6	−0.6	16.5 ± 0.3
$SG[M]_{F6}M$	2.4	−19.7	5.4	1.6	6.8	−0.9	21.3 ± 0.5

[a] The activation energy (E_a) is equal to the free energy difference between the first well and the first barrier.

are called cage holes. The difference between the two is that cage faces can prevent methane from crossing them whereas cage holes cannot. The so-called face-saturated cages do not contain any holes. The present results (Figure 5) confirm that the above definition is theoretically reasonable. It implies that a cage structure must be self-enclosed to ensure the basic function of keeping guests from entering or leaving the cage.

The findings in this work also have implications for the inter-cage diffusion of methane in hydrate. If the hydrate is crystalline, methane diffusion cannot occur unless some 5- and 6-membered faces break down [30]. However, if the hydrate is amorphous, the situation is different because the amorphous hydrate contains some opening cages with 7-membered holes [15,17]. Two opening cages can fuse together via the 7-membered hole to form a complex self-enclosed cage (see Supplementary Figure S6 in Ref. [17]), and methane can diffuse across the hole without breaking other faces.

5. Conclusions

In this work, we investigate the effects of cage type and adsorption face on the cage–methane adsorption interaction. We find that cage types have almost no effect on the interaction, except that the incomplete A cage shows a slightly weaker attraction to methane than do the other complete cages. However, the size of the adsorption face has a strong effect on the cage–methane adsorption. When the face size is increased from 4 to 6, the first well of the PMF shifts closer to the adsorption face and becomes deeper. This shows that a larger face attracts the dissolved methane more strongly, and thus implies that a preferential direction of cage development may exist during hydrate nucleation and growth. However, once the face is 7-membered or more, it can no longer adsorb methane and actually transforms into a hole that allows the methane to enter the cage. This finding provides a solid foundation for our recently established cage identification method (i.e., FSICA), and strengthens the idea that a water cluster can be distinguished as a cage because it is self-enclosed to its guests. In our next study, we will investigate the effects of different guest molecules such as CO_2, H_2, C_2H_6, C_3H_8, and THF, and inert gas molecules such as He, Ne, Ar, Kr, and Xe on the cage-guest adsorption interaction.

Acknowledgments

We thank the Computer Simulation Lab at IGGCAS for allocation of computing time. This work was financially supported by the National Basic Research Program of China (Program 973, Grant No. 2009CB219503), the Chinese Academy of Sciences (Grant No. KZCX2-EW-118), and the National Natural Science Foundation of China (Grant No. 41020134003).

Appendix A. Supplementary data

Supplementary data associated with this article can be found, in the online version, at http://dx.doi.org/10.1016/j.cplett.2013.05.012.

References

[1] E.D. Sloan, C.A. Koh, Clathrate Hydrates of Natural Gases, third ed., CRC Press, Boca Raton, 2008.
[2] C.A. Koh, E.D. Sloan, AIChE J. 53 (2007) 1636.
[3] R. Ohmura, M. Ogawa, K. Yasuoka, Y.H. Mori, J. Phys. Chem. B 107 (2003) 5289.
[4] P.W. Wilson, A.D.J. Haymet, Chem. Eng. J. 161 (2010) 146.
[5] C.A. Koh, Chem. Soc. Rev. 31 (2002) 157.
[6] P. Buchanan, A.K. Soper, H. Thompson, R.E. Westacott, J.L. Creek, G. Hobson, C.A. Koh, J. Chem. Phys. 123 (2005) 164507.
[7] J.M. Schicks, J.A. Ripmeester, Angew. Chem., Int. Ed. 43 (2004) 3310.
[8] M.R. Walsh, J.D. Rainey, P.G. Lafond, D.-H. Park, G.T. Beckham, M.D. Jones, K.-H. Lee, C.A. Koh, E.D. Sloan, D.T. Wu, A.K. Sum, Phys. Chem. Chem. Phys. 13 (2011) 19951.
[9] R.L. Christiansen, E.D. Sloan, Ann. N. Y. Acad. Sci. 715 (1994) 283.
[10] R. Radhakrishnan, B.L. Trout, J. Chem. Phys. 117 (2002) 1786.
[11] G.-J. Guo, M. Li, Y.-G. Zhang, C.-H. Wu, Phys. Chem. Chem. Phys. 11 (2009) 10427.
[12] R.W. Hawtin, D. Quigley, P.M. Rodger, Phys. Chem. Chem. Phys. 10 (2008) 4853.
[13] M.R. Walsh, C.A. Koh, E.D. Sloan, A.K. Sum, D.T. Wu, Science 326 (2009) 1095.
[14] L.C. Jacobson, W. Hujo, V. Molinero, J. Am. Chem. Soc. 132 (2010) 11806.
[15] J. Vatamanu, P.G. Kusalik, Phys. Chem. Chem. Phys. 12 (2010) 15065.
[16] G.-J. Guo, Y.-G. Zhang, H. Liu, J. Phys. Chem. C 111 (2007) 2595.
[17] G.-J. Guo, Y.-G. Zhang, C.-J. Liu, K.-H. Li, Phys. Chem. Chem. Phys. 13 (2011) 12048.
[18] J.S. Loveday, R.J. Nelmes, M. Guthrie, Chem. Phys. Lett. 350 (2001) 459.
[19] H. Tanaka, Y. Amano, Mol. Phys. 100 (2002) 2183.
[20] E. Lindahl, B. Hess, D. van der Spoel, J. Mol. Model. 7 (2001) 306.
[21] D. van der Spoel, E. Lindahl, B. Hess, A.R. van Buuren, E. Apol, P.J. Meulenhoff, D.P. Tieleman, A.L.T.M. Sijbers, K.A. Feenstra, R. van Drunen, H.J.C. Berendsen, Gromacs User Manual, version 4.0.7, www.gromacs.org, 2009.
[22] J.L.F. Abascal, C. Vega, J. Chem. Phys. 123 (2005) 234505.
[23] W.L. Jorgensen, J.D. Madura, C.J. Swenson, J. Am. Chem. Soc. 106 (1984) 6638.
[24] H. Docherty, A. Galindo, C. Vega, E. Sanz, J. Chem. Phys. 125 (2006) 074510.
[25] M.M. Conde, C. Vega, J. Chem. Phys. 133 (2010) 064507.
[26] R. Sun, Z. Duan, Geochim. Cosmochim. Acta 69 (2005) 4411.
[27] E.A. Mastny, C.A. Miller, J.J. de Pablo, J. Chem. Phys. 129 (2008) 034701.
[28] F.W. Starr, J.K. Nielsen, H.E. Stanley, Phys. Rev. Lett. 82 (1999) 2294.
[29] Y.F. Makogon, Ann. N. Y. Acad. Sci. 715 (1994) 119.
[30] B. Peters, N.E.R. Zimmermann, G.T. Beckham, J.W. Tester, B.L. Trout, J. Am. Chem. Soc. 130 (2008) 17342.